

Prospects of hard X-ray polarimetry with Astrosat-CZTI

T. Chattopadhyay · S. V. Vadawale · A. R. Rao ·
S. Sreekumar · D. Bhattacharya

Received: 31 January 2014 / Accepted: 3 April 2014 / Published online: 9 May 2014
© Springer Science+Business Media Dordrecht 2014

Abstract Astrosat is the first Indian satellite mission dedicated for astronomical studies. It is planned for launch during 2014 and will have five instruments for multi-wavelength observations from optical to hard X-rays. Cadmium Zinc Telluride Imager (CZTI) is one of the five instruments aiming for simultaneous X-ray spectroscopy and imaging in the energy range of 10 keV to 100 keV (along with all sky photometric capability upto 250 keV). It is based on pixilated CZT detector array with total geometric area of 1024 cm^2 . It will have two-dimensional coded mask for medium resolution X-ray imaging. The CZT detector plane will be realized using CZT detector modules having integrated readout electronics. Each CZT detector module consists of $4 \text{ cm} \times 4 \text{ cm}$ CZT with thickness of 5 mm which is further pixilated into 16×16 array of pixels. Thus each pixel has size of $2.5 \text{ mm} \times 2.5 \text{ mm}$ and thickness of 5 mm. Such pixilated detector plane can in principle be used for hard X-ray polarization measurements based on the principle of Compton scattering by measuring azimuthal distribution of simultaneous events in two adjacent pixels. We have carried out detailed Geant4 simulations for estimating polarimetric capabilities of CZTI detector plane. The results indicate that events in the energy range of

T. Chattopadhyay (✉) · S. V. Vadawale
Astronomy and Astrophysics Division, Physical Research Laboratory,
Ahmedabad, India
e-mail: tanmoy@prl.res.in

A. R. Rao
Department of Astronomy and Astrophysics, Tata Institute of Fundamental Research,
Mumbai, India

S. Sreekumar
Baseband Systems Electronics Division, Vikram Sarabhai Space Centre,
Thiruvananthapuram, India

D. Bhattacharya
The Inter-University Centre for Astronomy and Astrophysics, Pune, India

100 keV to 250 keV, where the 5 mm thick CZT detector has significant detection efficiency, can be used for polarimetric studies. Our simulation results indicate the minimum detectable polarization (MDP) at the level of $\sim 10\%$ can be achieved for bright Crab like X-ray sources with exposure time of ~ 500 ks. We also carried out preliminary experiments to verify the results from our simulations. Here we present detailed method and results of our simulations as well as preliminary results from the experimental verification of polarimetric capabilities of CZT detector modules used in Astrosat CZTI.

Keywords X-ray polarimetry · Instrumentation · Compton scattering · Astrosat-CZT imager

1 Introduction

Polarization measurement of X-rays from celestial X-ray sources is expected to give unique insights on physical mechanisms and the geometries of X-ray sources in the extreme magnetic and gravitational fields. However, because of extremely photon hungry nature of X-ray polarimetry, resulting in low sensitivity of X-ray polarimeters, it has largely remained unexplored so far. Apart from some initial attempts in 1970s [7, 8, 12, 18, 20, 27] no dedicated polarimetric experiments were conducted during last 40 years. With recent improvement in detection technology, many groups across the globe are trying to develop sensitive X-ray polarimeters both in soft X-rays based on photo-electron imaging technique [4, 13] and in hard X-rays based on Compton scattering technique [2, 3, 9, 19, 21, 23, 28]. In the absence of dedicated polarimeters, there have been a few attempts to extract the polarimetric information with the available data from existing spectroscopic and imaging instruments such as INTEGRAL-IBIS [15], INTEGRAL-SPI [5] by utilizing their pixilated nature. Such pixilated detectors can in principle work as Compton polarimeters if they have capability to detect and record simultaneous events occurring in multiple pixels. Thus, in order to expand the so far limited field of X-ray polarimetry, apart from attempting optimised X-ray polarization experiments, the possibility of extracting polarimetric information from any pixilated detector should always be explored whenever possible.

One of such instruments employing large pixilated CZT detector plane is the CZT-Imager (CZTI) onboard Astrosat - the forth-coming Indian astronomy mission. CZT detectors are considered as workhorse for the hard X-ray astronomy because of its high efficiency and resolution at those energies [10, 17, 24, 25]. Astrosat-CZTI is an imaging instrument using a coded mask and consists of total 1024 cm^2 pixilated CZT detector array for hard X-ray imaging and spectroscopy in the 10 keV to 100 keV range. The detector plane of CZTI is composed of total 64 CZT detector modules having integrated readout ASIC. The modules are procured from Orbotech Medical Solutions. Each module is $4 \text{ cm} \times 4 \text{ cm}$ in dimension and thickness is 5 mm and is further pixilated in array of 16×16 pixels of dimension $2.5 \text{ mm} \times 2.5 \text{ mm}$ (see Fig. 1). Time resolution of CZTI is $20 \mu\text{s}$. Further details of Astrosat-CZTI can be found in [1].

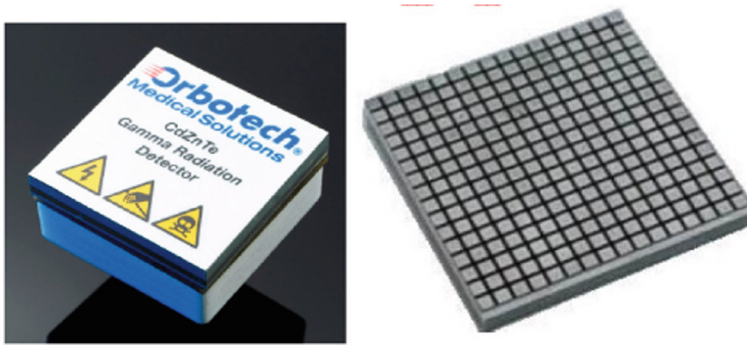


Fig. 1 *Left* A single CZTI module procured from Orbotech Medical Solutions. Dimension of the module is 40 mm × 40 mm. Thickness is 5 mm. *Right* CZTI module is pixelated into an array of 16 × 16 pixels, therefore pixel size of 2.5 mm

Though this configuration of CZTI in principle should be capable of polarization measurement, feasibility of Compton polarimetry with CZTI depends on many other factors e.g.

- Whether the Orbotech CZTI modules have multi-pixel detection capability or not,
- If the modules do have multi-pixel detection capability then whether CZTI will have any meaningful polarimetric sensitivity
- Lastly, whether the polarimetric information is preserved by the onboard data processing.

We experimentally verified the multi-pixel capability of the Astrosat CZTI modules and carried out detailed Geant4 simulation for such a pixelated CZT detectors to estimate the polarimetric sensitivity of Astrosat CZTI. We also carried out preliminary experiments to verify the capability of the CZTI processing electronics to preserve the polarimetric information. Here we present the simulation results in detail and describe the experimental results.

2 Compton polarimetry with pixelated detectors

When a polarized beam of X-ray photons is Compton scattered, it is preferentially scattered perpendicular to the direction of polarization, cross-section of which is given by the Klein Nishina formula [11]

$$\frac{d\sigma_C}{d\Omega} = \frac{r_e^2}{2} \left(\frac{E'}{E} \right)^2 \left[\frac{E'}{E} + \frac{E}{E'} - 2 \sin^2 \theta \cos^2 \phi \right] \quad (1)$$

where E and E' are the energy of the incident and scattered photon respectively corresponding to scattering angle θ . ϕ is the azimuthal angle of scattering. r_e is classical electron radius. The azimuthal angle is measured with respect to the polarization vector and we can see that the azimuthal angle of scattering is modulated with a $\cos^2 \phi$

term with the modulation amplitude directly proportional to polarization fraction of the incident beam. The above equation can be re-written as (using an explicit term ϕ_0 for the polarization angle)

$$C(\phi) = A \cos(2(\phi - \phi_0 + \frac{\pi}{2})) + B \quad (2)$$

where A and B are the fitting parameters and are used to estimate the modulation factor, μ

$$\mu = \frac{A}{B} \quad (3)$$

Polarization fraction being proportional to the modulation factor, one can obtain the degree of polarization of the beam from (3). Polarimetric sensitivity is given in terms of Minimum Detectable Polarization (MDP) at 99 % confidence limit,

$$MDP_{99\%} = \frac{4.29}{\mu_{100} R_{src}} \sqrt{\frac{R_{src} + R_{bkg}}{T}} \quad (4)$$

where R_{src} and R_{bkg} are the source and background count rates. T is the exposure time and μ_{100} is the modulation factor for 100 % polarized beam. Geometry of a Compton polarimeter basically employs low Z active scatterer(s) surrounded by an array of absorbers of high Z elements. From the simultaneous events between scatterer and absorber, azimuthal angle distribution is obtained which is then used to estimate the modulation factor and polarization angle. Sensitivity of the polarimeters can be increased either by increasing μ_{100} which depends on the geometry of the polarimeter (range in scattering angle of the photons) or by increasing the number of detected photons (R_{src}) by pushing down the threshold of the scatterer as much as possible.

Compton polarimetry with pixilated detectors works on the same principle. Here the double pixel events arising from the Compton scattering of a photon in one pixel and absorption of the scattered photon in another pixel constitute the basic polarization event. The azimuthal angle of the Compton scattering is determined from the direction of center of the scattering pixel to the center of the absorbing pixel with reference to a pre-defined instrument reference plane. The histogram of the azimuthal angle distribution can then be used to determine modulation factor and polarization angle as usual. It is to be noted that in case of pixilated detectors, the azimuthal angle bins are unequal which leads to an inherent modulation pattern in the azimuthal angle distribution. Thus the observed modulation pattern has to be normalized using the similar modulation pattern for unpolarized beam as discussed later.

Astrosat-CZTI consists of an array of pixilated CZT detectors with pixel size of 2.5 mm. Timing resolution of CZTI being 20 μ s, simultaneous events can be determined with minimum of 20 μ s time window. As the CZT detectors with 5 mm thickness has significant Compton scattering efficiency at energies > 100 keV, it is expected that Astrosat-CZTI can provide useful polarization measurement at energies even beyond its primary energy range. This aspect is particularly important because at energies > 100 keV, the coded mask and other support structure of CZTI becomes increasingly transparent making almost full area of 1024 cm² available for the Compton polarimetry.

3 Multi-pixel detection capability of CZTI detector modules

3.1 Experiment set up

In order to verify multi-pixel capability of CZTI modules, we conducted an experiment in which 1 CZTI module was illuminated with a partially polarized beam of energy ~ 100 keV.

The experiment setup is shown in Fig. 2. Polarized beam of 100 keV photons was produced by Compton scattering of 122 keV line of ^{57}Co from a plastic scatterer constraining the angle of scattering at 90° . Scatterer, placed in front of ^{57}Co is 6 cm in length. Both the plastic scatterer and source are kept inside a thick lead (thickness 2 cm) cylinder with a narrow slit of dimension $5\text{ cm} \times 5\text{ mm}$. CZTI module was kept at angle 90° with respect to the axis of cylinder as shown in Fig. 2. Alignment of the slit and the CZTI module was carefully done from the pixel image of the module.

Since, radioactivity is a random phenomenon, time interval between two successive independent events recorded in CZTI module can be modeled by Poisson's statistics. However, Compton scattering of an incident photon results in multiple interactions due to the deposited energies in Compton scattering and subsequent absorption of the scattered photon, either in the same pixel or separate pixels. These events, being correlated to each other, should deviate from the modeled Poisson's distributed time intervals.

3.2 Data analysis and results

Figure 3 shows the histogram of time intervals between two successive events. There is clearly an excess of events with time interval below $40\ \mu\text{s}$ beyond which the ΔT

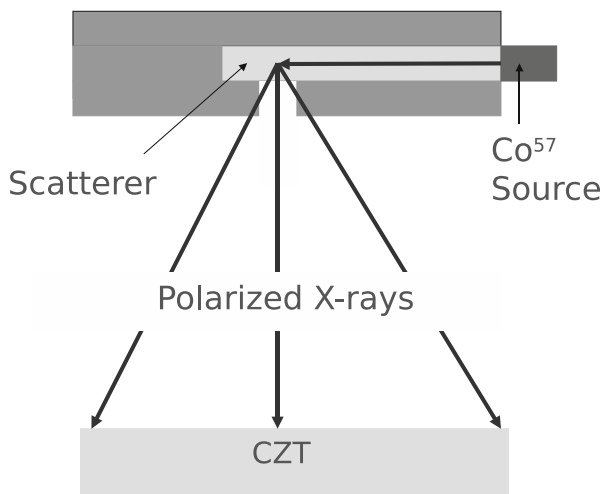


Fig. 2 Schematic Diagram of the experiment setup. 122 keV photons from ^{57}Co are scattered at 90° by a plastic scatterer and interact with CZTI module

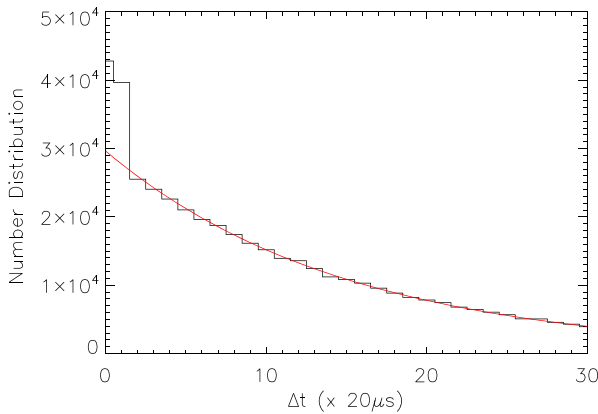


Fig. 3 Distribution of time intervals of all successive events recorded in CZTI module in ^{57}Co experiment. There is an excess of events for time interval below $40\ \mu\text{s}$. The events beyond $40\ \mu\text{s}$ time interval have been fit with a Poisson's function shown by *solid red line*

distribution agrees nicely with the Poisson's distribution. Each event has an individual time stamp with a resolution of $20\ \mu\text{s}$. Any two events recorded within duration of $20\ \mu\text{s}$ will have the same time stamp. Therefore the genuine multi-pixel events i.e. those resulting from the Compton scattering or escape events in the photo-electric interaction should occur in the same time bin of $20\ \mu\text{s}$. We observe significant excess in the second time bin (events occurring between $20\ \mu\text{s}$ to $40\ \mu\text{s}$), however, this is due to the specific read-out logic implemented in the CZTI and is well understood. The detector modules can detect multi-pixel events and store them internally. The time stamp to each event is assigned to after being read-out. Since the read-out logic is configured to read event from one module at a time, it is quite possible that two simultaneous events in different pixels of a given module may get two consecutive time stamps, which results in excess events in the second bin of the ΔT distribution. Thus we believe that a large fraction of the excess events recorded within $40\ \mu\text{s}$ are true simultaneous events. We have repeated the same experiment with other modules and find similar results. This clearly shows that the CZTI modules do have capability to detect and record multiple simultaneous events.

It should be noted that $40\ \mu\text{s}$ is significantly large duration for being considered as simultaneous and thus could result in many chance coincidence events. In fact, we do observe successive events in the same pixel with two consecutive time stamps which are clearly chance events. In order to properly identify such chance events and ignore them, we check time stamps of up to five events at a time (we start with one event and compared the time stamp, t_i , of that event with time stamps of next subsequent events, t_{i+1} , t_{i+2} ..., until the difference in time arrival is $> 40\ \mu\text{s}$) and list all double, triple or more pixel events. We do find a small fraction of three (or even four) pixel events occurring within $40\ \mu\text{s}$, however all such events are ignored and only double pixel events are considered for further analysis. Fig. 4 shows the spectra for the valid double pixel events. Each valid event involves two pixels; in case of Compton scattering, the pixel with less deposited energy is the primary pixel and the

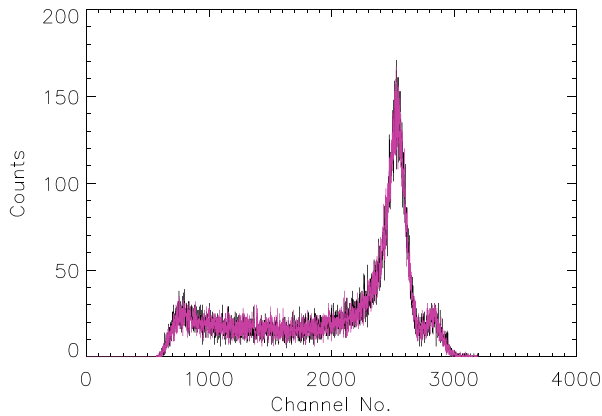


Fig. 4 Spectra obtained for all double pixel events from ^{57}Co experiment. *Black* and *red* refer to two pool of pixels. For details, refer to text

other one is the secondary pixel. However, since the module is illuminated uniformly, it is not possible to identify primary and secondary pixels a priori. Hence, channel histogram for both the pixels, denoted by black and red, is shown in Fig. 4.

This spectra appears similar to the spectra obtained by the direct exposure of X-rays from ^{57}Co , with both the peaks corresponding to the 122 keV and 136 keV lines clearly visible. This is because of the fact that all double pixel events are dominated by the chance coincidence events, occurring due to relatively large coincidence window of 40 μs , of widely separated and independent single pixel events. Since the Compton scattered photon is not expected to travel far from the scattering pixel before getting absorbed, we consider double pixel events occurring only within the adjacent pixels to avoid the chance coincidence events. Top panel of Fig. 5 shows the spectra of the two pixels for all adjacent double pixel events. It can be seen that majority of chance coincidence events, manifested by the 122 keV and 136 keV peaks, are now absent. However, a small fraction of such events are still present. To prevent even this small fraction of the chance coincidence events, we impose another condition on the ratio of the energy deposited in the two pixels of the adjacent double pixel events. For a true Compton scattering event, energy of the scattered photon is always greater than the recoil electron energy for incident photon energies < 280 keV, even for maximum scattering angles. For lower energy of the incident photons and scattering angles around 90° , the ratio of the energy of the scattered photon and the recoil electron is ≥ 2 . Therefore, we consider only those adjacent double pixel events which satisfy this condition. Bottom panel of Fig. 5 shows spectra of both pixels after applying the ratio condition. This is the graphical representation of the multi-pixel detection capability of the CZTI modules. It can be seen that the ratio condition is also helpful in rejecting other chance events arising from the electronic noise. The first peak in the spectra corresponds to the primary Compton scattering pixels and the second peak corresponds to the absorption of the scattered photons.

It should be noted, however, that these events may not be pure Compton scattering events as the escape photons from CZT can also mimic the Compton scattering

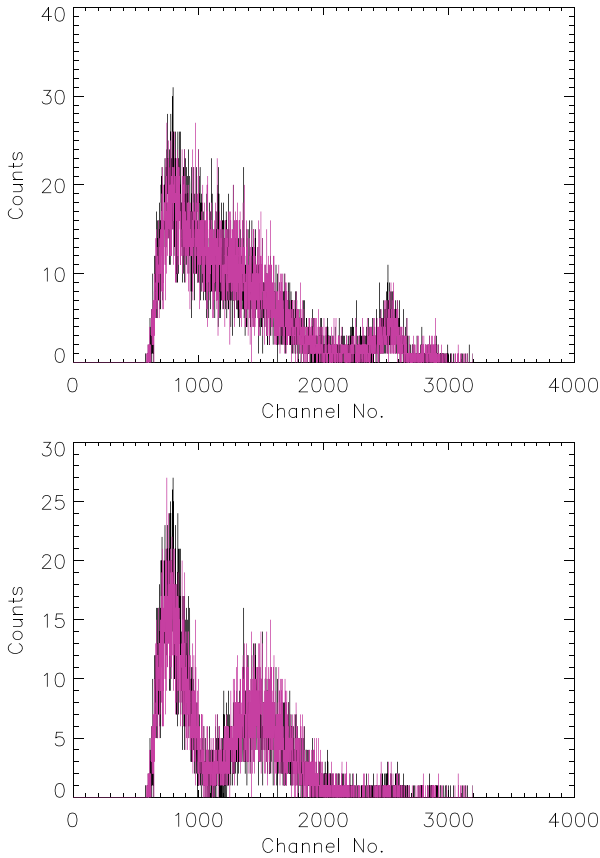


Fig. 5 *Top* Spectra for the neighboring double pixel events. *Bottom* spectra obtained after applying ratio condition (ratio of deposited energies ≥ 2) on the neighboring double pixel events

and hence the same distribution is also possible for the double pixel events arising from the detection of the escape photons. In order to estimate the fraction of such events and estimate polarimetric sensitivity of CZTI, we carried out detailed Geant4 simulation as described in the following section.

4 Geant4 simulation

We used Geant4 toolkit [6] to estimate modulation factor and efficiency of a single CZTI module for 100 % polarized beam. CZTI module's electronics ULD is around 250 keV. For a 5 mm thick CZT, probability of Compton scattering becomes significant beyond 100 keV. So, simulation was done for mono-energetic 100 % polarized and unpolarized beams in the energy range of 100 keV to 300 keV, employing low energy electromagnetic processes e.g. *G4LowEnPolarizedPhotoElectric*, *G4LowEnPolarizedRayleigh*, *G4LowEnPolarizedCompton*, *G4LowEnBremss* and

G4LowEnIonization. The incident beam of photons was generated using General Particle Source (GPS) which was perpendicularly incident on a single CZT block (40 mm \times 40 mm \times 5mm) as shown in Fig. 6. For each energy, we carried out simulation for 10 million photons incident on CZT uniformly across its surface and for each energy, the polarization angle was varied from 0° to 90° at a step of 11.25°. For each photon, maximum of 7 secondary photon interaction positions and corresponding deposited energies were recorded. Deposited energy for each of such interactions is calculated by summing up the individual energies of all the secondary electrons generated in that interaction. We ignore the electron track lengths and assume that total energy of the secondary electron is deposited at the location of the photon interaction. Output is kept in the form of an event list with different types of interactions, positions of interactions (maximum 7), energy deposited in each interaction etc.

4.1 Estimation of polarimetric efficiency

Further data analysis was done using IDL (Interactive Data Language). Since pixel size of *Astrosat-CZTI* modules is 2.5 mm, the interaction positions in the event list are pixilated with 2.5 mm spacing. For multiple photon interactions occurring within the boundary of a single pixel, energies deposited in these interactions are added together to get the total energy deposition in the given pixel. In this way, we divide all events in single pixel, double pixel, three pixel up to maximum 7 pixel events. Figure 7 shows the probabilities of the single, double and multiple pixel (≥ 3) events as a function of incident photon energies. As only the double pixel events are useful for the polarization measurement, further analysis is carried out only for the double pixel events. Figure 8 shows the probability of different types of interactions giving rise to the double pixel events. We see that apart from the valid Compton scattering events (1 Compton and 1 photoelectric) providing the polarimetric information, there are many

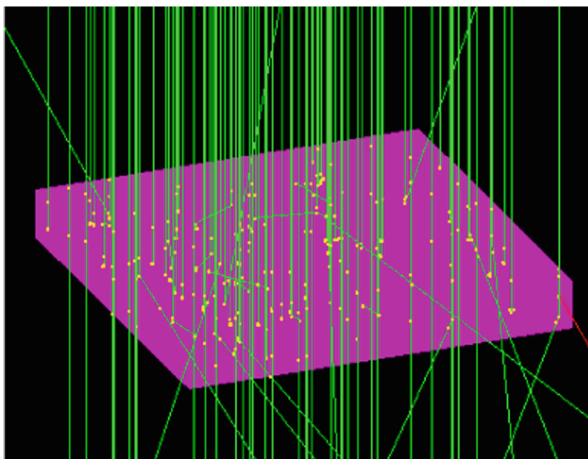


Fig. 6 Simulated diagram for a CZT module (40 mm \times 40 mm \times 5mm). The module is shined uniformly by X-ray photons shown in green

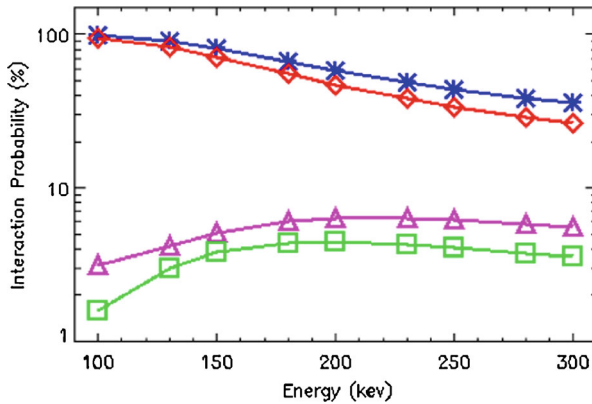


Fig. 7 Probability of single pixel (*red, diamond*), double pixel (*pink, triangle*) and greater than double pixel events (*green, square*) as a function of photon energies for 2.5 mm pixel size. Total interaction probability for 5 mm thick CZT is shown in blue (*asterisks*)

other types of double pixel events which may contaminate the azimuthal distribution of the real Compton scattering events and blur the polarization signature embedded in the incident beam. Pure photoelectric events (shown in blue) are because of detection of an incident photon in one pixel due to photoelectric absorption and detection of the consequent escape photon (~ 30 keV) in another pixel. Probability of these events is quite significant ($\sim 1\%$). On the other hand, a photoelectric absorption may lead to bremsstrahlung photons from the ejected electron, detection of which may trigger double pixel events (shown in yellow and light blue). All these events may mimic the true Compton scattering events and jeopardise the polarization signature in the beam.

To obtain spectra for these double pixel events, we assumed the pixel with lower energy deposition to be the primary pixel i.e. where the Compton scattering takes place and the pixel with higher energy deposition to be the secondary pixel in which

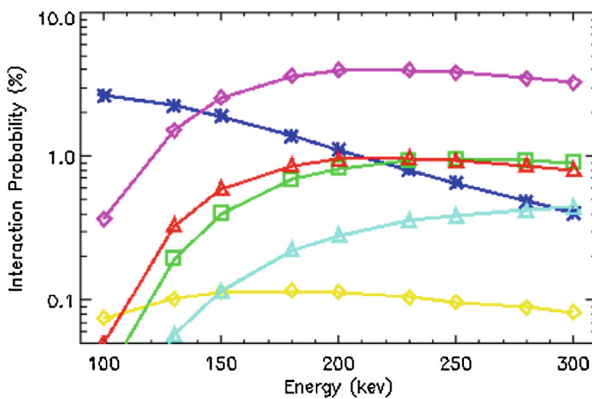


Fig. 8 Different processes generating double pixel events: photo-photo (*blue, asterisks*), 1compt-photo (*pink, diamond*), 1compt-1photo (*red, triangle*), photo-multi compt (*green, square*), photo-brem (*yellow, diamond*), photo-brem-compt (*light blue, triangle*)

the scattered photon is absorbed. This assumption holds good for incident photons with energies up to 280 keV. Representative spectra of true Compton events and other double pixel events for the incident photons of 200 keV are shown in Fig. 9. Spectra shown in black and blue are for primary and secondary pixels respectively. Spectra for pure photoelectric events shows two peaks at lower and higher energies due to escape photons. The upper left panel shows spectra of double pixel events of ideal Compton events and the upper right panel shows spectra of all double pixels events with minimum energy deposition above the detection threshold (20 keV) i.e. without any selection on interaction type. The bottom panels show spectra for only photoelectric escape events (left) and photoelectric+bremsstrahlung events (right). It should be noted that these are the spectra of only deposited energy in the pixels and are not convolved for the CZT detector response.

4.2 Estimation of modulation factor

Using pixel map for the double pixel events, we obtained the azimuthal angle for each of the events. Representative azimuthal distribution corresponding to the incident photon energy of 200 keV and polarization angle of 0° are shown in Fig. 10, where the top panel shows the azimuthal angle distribution for ideal Compton events (1 Compton and 1 photoelectric) and the bottom panel shows the same for all double pixel events with 20 keV threshold in the CZTI module. It is to be noted that azimuthal angle distribution has an inherent modulation pattern due to the unequal

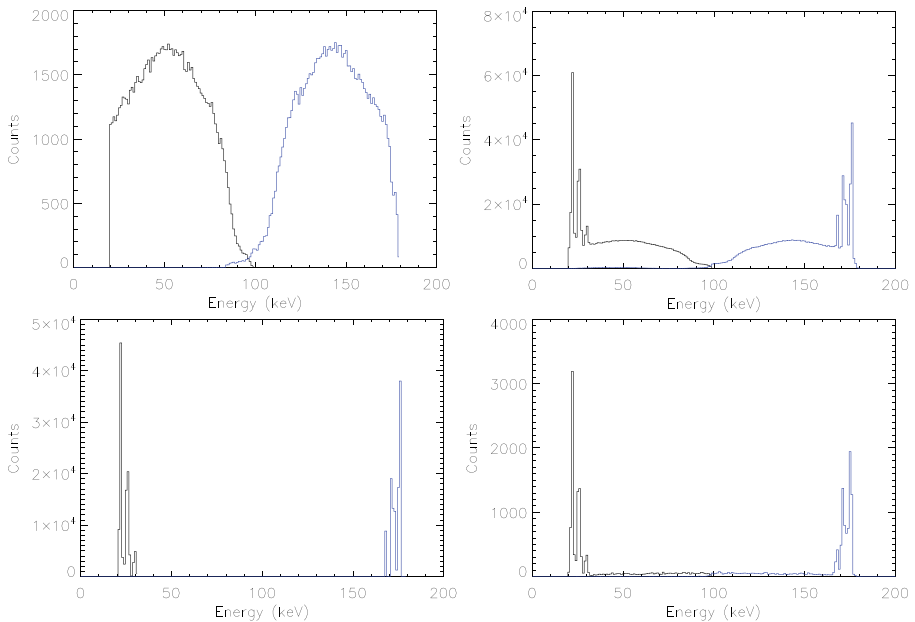


Fig. 9 Spectra obtained from simulation of 200 keV beam. *Black and blue* refer to primary and secondary pixels respectively. *Top-left* ideal Compton events; *Top-right* all double pixel events; *Bottom-left* photoelectric escape events; *Bottom-right* photoelectric-bremsstrahlung events

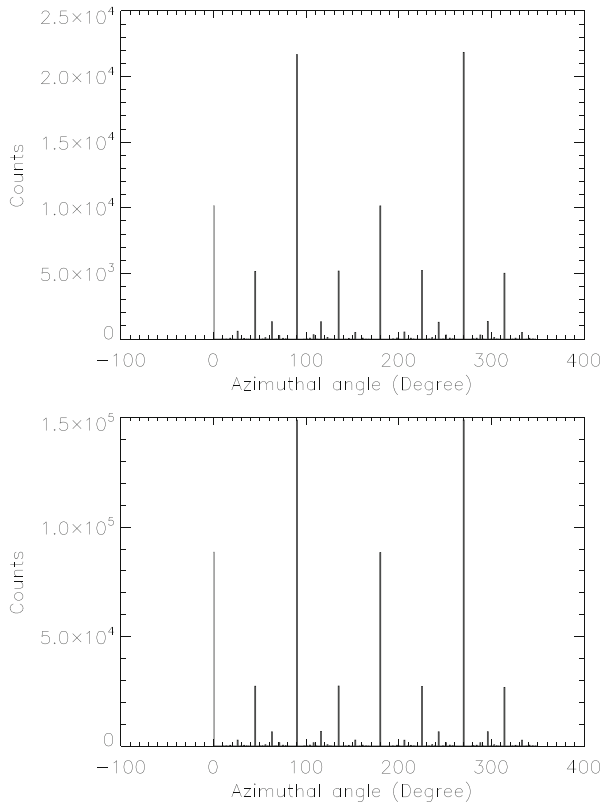


Fig. 10 Azimuthal angle distribution for 200 keV beam with polarization angle of 0° . *Top* ideal Compton events. *Bottom* all double pixel events with 20 keV threshold

bin size with respect to the primary pixel i.e. the azimuthal angle covered by the edge pixels is much larger than that for corner pixels and hence more number of photons are detected in edge pixels. Since the polarization direction is parallel to the direction of edge pixels, the counts in the edge pixels are modulated whereas for corner pixels have the same average number of counts. Modulation factor in this case (0° polarization angle) can be estimated from the events corresponding to 0° and 90° bins or 180° and 270° bins. Estimated modulation factor for the ideal Compton events is, $\mu = 0.36$, whereas for all the double pixel events it is, $\mu = 0.25$. The modulation factor for all events is clearly degraded compared to the true Compton events due to the false events arising because of photoelectric and bremsstrahlung interactions.

In the previous section, we discussed two conditions derived from the experimental data i.e. considering only adjacent pixel events and ratio of scattered to deposited energy ≥ 2 . In order to get realistic estimate of the modulation factor from the simulated data, we apply the same conditions to the simulated double pixel events without using the knowledge of the underlying interactions. Figure 11 shows the spectra and azimuthal angle distribution for the double pixel events on the basis of these conditions. It can be seen that the modulation factor after applying these two conditions,

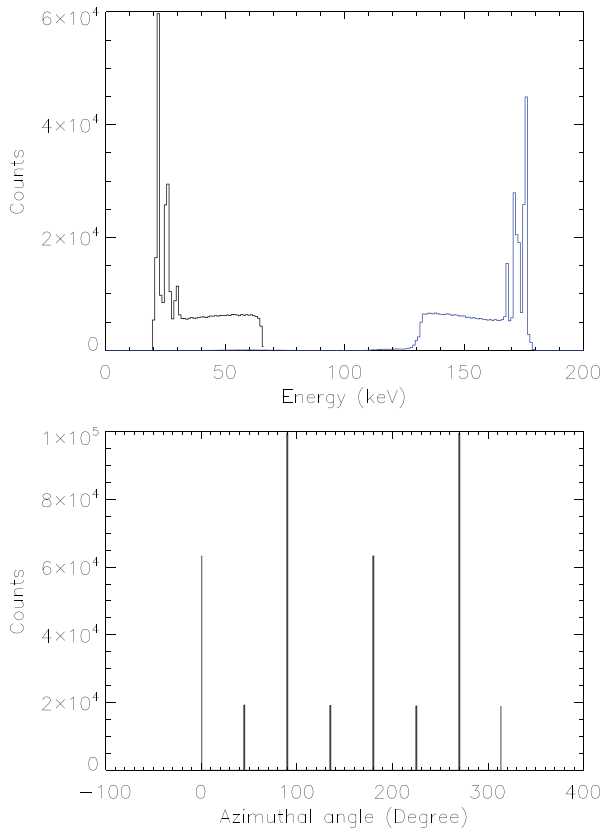


Fig. 11 Spectra (*top*) and azimuthal angle distribution (*below*) obtained from simulation of 200 keV beam (polarization angle of 0°) considering the adjacent double pixel events including the criteria of ratio of deposited energies greater than 2

$\mu = 0.23$, has slightly degraded from the original modulation factor obtained by including all events into calculation. This is because of the second condition of ratio of energy deposited in two pixels to be ≥ 2 , which actually rejects some valid Compton events where the scattering angle is greater than $\sim 120^\circ$ as shown in Fig. 12. This in turn introduces assymetry in the range of scattering angle around 90° and thus the effective modulation degrades. Another negative effect of these conditions is to reduce the detection efficiency of the Compton events. However, both these conditions are essential in order to reduce other noisy events, as shown by the experimental data and hence the expected sensitivity is estimated using all these conditions.

It is to be noted that the overall degradation in modulation factor is mainly because of the escape photons which may be avoided by applying energy threshold of 35 keV in both primary and secondary pixels. With this condition the modulation factor increases from 23 to 41 % at 200 keV for polarization angle of 0° . However, this condition restricts the lower energy detection limit of polarization to be around 150 keV (see Fig. 13), thereby reduces the overall polarimetric sensitivity of the instrument.

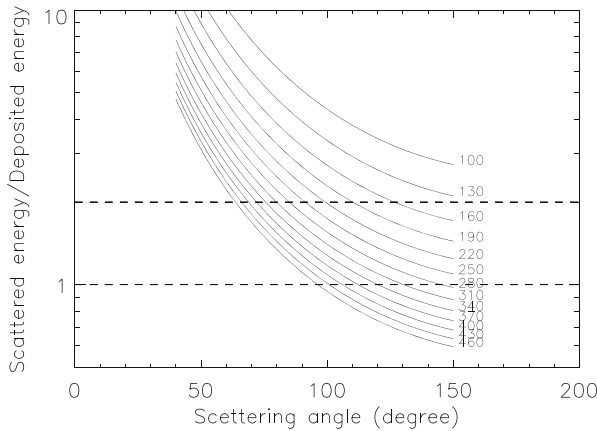


Fig. 12 Ratio of Compton scattered photon energy to electron recoil energy as a function of scattering angle and incident photon energies. The photon energies mentioned in the plot are in keV unit

As mentioned earlier, the azimuthal bins are asymmetric for the pixilated detectors and hence the azimuthal distribution has inherent modulation pattern. This inherent modulation pattern can be corrected by normalizing the azimuthal distribution with respect to the azimuthal distribution for unpolarized beam at the same energy (or energy range) [14, 16]. If $N_{i,pol}$ is the number of counts in i^{th} bin for 100 % polarized beam and $M_{i,unpol}$ is the counts in that bin for 100 % unpolarized beam with average number of counts in each bin \bar{M}_{unpol} , then normalised counts in i^{th} bin will be

$$N_{i,corrected} = \frac{N_{i,pol}}{M_{i,unpol}} \bar{M}_{unpol} \tag{5}$$

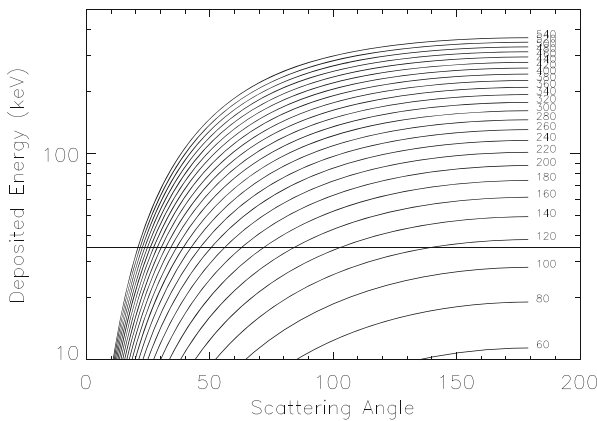


Fig. 13 Deposited energy in Compton scattering as a function of scattering angle and incident photon energies. The incident photon energies for each line mentioned in the plot are in keV unit. For incident energies greater than 140 keV, deposited energy is greater than 35 keV

Fig. 14 shows the modulation curves at 200 keV for different polarization angles after correcting for the geometry using (5). The modulation curve is fitted by (2) and the fitting parameters are used to estimate the modulation factor (see (3)). There are few points to be noted - 1) Modulation factor does not depend on geometric correction. 2) Modulation factor is higher for 45° polarization angle because, photons are restricted to be scattered close to 90° because of the geometry. 3) Modulation factor is polarization angle dependent which implies that the sensitivity of the instrument too will depend on the angle of polarization of the beam with respect to the instrument reference plane. It is obvious that in real life situation, the plane of polarization of the incident X-rays will not be known. Therefore, the dependence of polarization measurement on the incident polarization angle means that X-ray polarization for any celestial source measured by Astrosat-CZTI must be verified at different instrument angles with reference to the measured polarization angle. This can be achieved either by the rotation of the spacecraft with respect to the source direction or by observing the same source at different time which may have different spacecraft position with respect to the source. Another important point to note is that the geometric correction in the raw azimuthal angle distribution introduces an additional statistical uncertainty in the modulation factor. As the azimuthal angle distribution of the unpolarized photons can be estimated very accurately, the uncertainty in the corrected modulation factor is determined mainly from the statistical uncertainty of the observed azimuthal angle distribution. For sufficiently large number of unpolarized photons ($\sim 10^9$), we find that the uncertainty introduced by the correction is less than 0.3 %. However, this

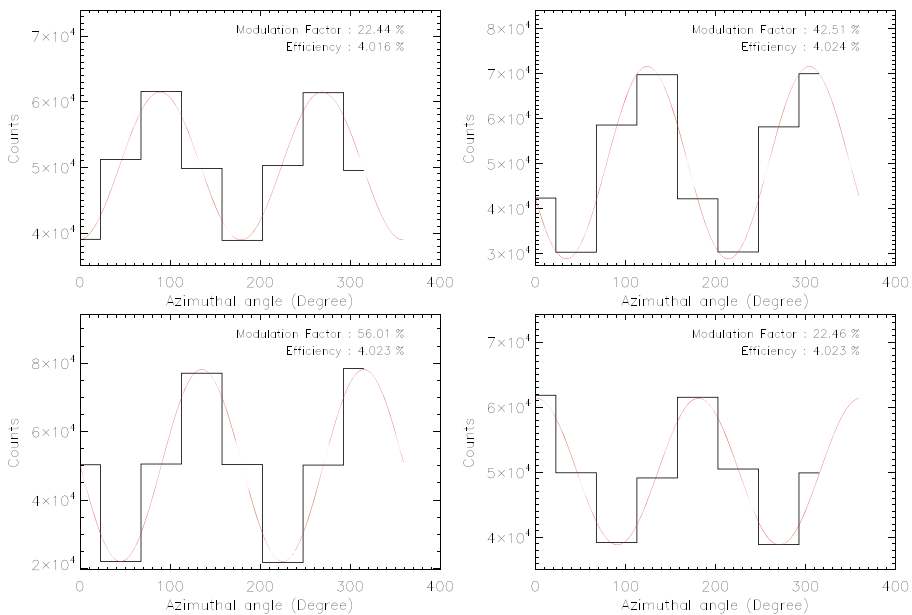


Fig. 14 Modulation curves at 200 keV for polarization angles (from upper left to lower right) of 0°, 22.5°, 45° and 90°. The modulation curves are fitted by the red solid lines (see (2)). Modulation factors and efficiencies for different polarization angles have been mentioned in the respective plots

additional uncertainty in modulation factor should be carefully taken into account because it sets the lower limit for the overall uncertainty in the measured polarization for any unknown beam.

Figure 15 shows the angle dependent modulation factors and detection efficiency as a function of incident photon energy. It can be seen that the modulation factor is maximum for 45° and minimum for 0° and 90° . Since scattering geometry is symmetric with respect to the polarization angles 0° and 90° , 11.25° and 78.75° so on, modulation factor is same at these polarization angles. Probability of photoelectric interaction being higher at lower energies, modulation factor is lower at those energies due to the dominance of the escape photons, compared to that at higher energies. Overall detection efficiency in the energy range of 100 to 300 keV is of the order of 3 % and does not depend on the polarization angle as expected.

5 Polarimetric sensitivity of ASTROSAT-CZTI

Polarimetric sensitivity of any X-ray polarimeter is customarily specified in terms of the Minimum Detectable Polarization (MDP) as given by (4). Thus estimation of MDP for Astrosat-CZTI require accurate knowledge of μ_{100} - the modulation factor for 100 % polarized X-rays, R_{bkg} - background count rate and R_{src} - source count rate, which in turn requires the knowledge of polarimetric detector efficiency in the energy range of interest. The modulation factor and the polarimetric detector efficiency are already determined from the Geant4 simulations (Fig. 15) in the energy range of 100 keV to 300 keV. The other quantities can be estimated as described in the following subsections.

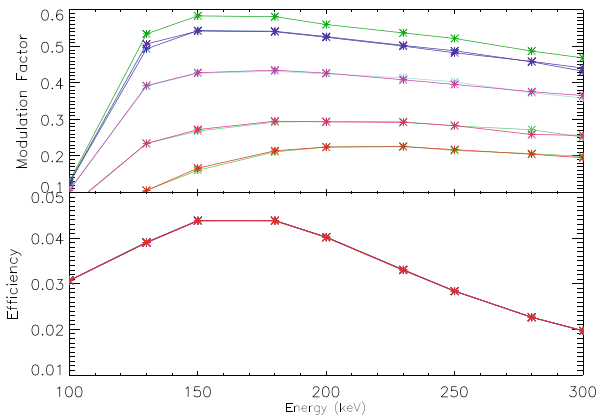


Fig. 15 Modulation factor and efficiency (for 100 % polarized beam) as a function of photon energy and polarization angle. Different polarization angles are denoted by different colors. In the modulation factor vs. energy plot, the curve at the top corresponds to 45° polarization angle. It is followed by 33.75° and 56.25° , 22.5° and 67.5° , 11.25° and 78.75° and 0° and 90° polarization angles respectively. Polarimetric efficiency is independent of polarization angle

5.1 Source count rate

Source count rate (R_{src}) can be estimated directly by integrating the source spectrum, which we assume to be Crab like for the present estimation over the effective collecting area of CZTI. As mentioned earlier, the polarimetric energy range of CZTI is beyond the primary spectroscopic energy range. Therefore the coded mask and other support structure of CZTI has significant transparency at those energies. Thus for an on-axis source, we estimate the total source count rate for the two cases - one for the open area of 512 cm^2 (50 % unobscured area of the coded mask) by integrating the source spectrum convolved with the polarimetric efficiency, and second for the area of 512 cm^2 shadowed by the partly transparent coded mask by integrating the source spectrum convolved with both the polarimetric efficiency and the transmission probability of the mask (made of 0.5 mm thick Tantalum). Following this method, the total count rate for the Crab is found to be $1.0006 \text{ cnt s}^{-1}$ in the energy range of 100 keV to 300 keV over the entire detector plane of the CZTI.

5.2 Background estimation

Estimation of background (R_{bkg}) for Astrosat-CZTI is more involved process. It should be noted that the polarimetric background of interest here is only the spurious double pixel events satisfying the filtering conditions mentioned in the previous section. Such spurious double pixel events can arise either from the chance coincidence of the usual spectroscopic background i.e. the instrumental background and the cosmic X-ray background (CXB) or these can also arise from the actual Compton scattering of the CXB photons. In either case, it is necessary to first estimate the spectroscopic background rate due to the cosmic X-ray background.

5.2.1 Cosmic X-ray background

Since Astrosat-CZTI has relatively wide field of view (FOV) of $6^\circ \times 6^\circ$, the cosmic X-ray background (CXB) within the FOV has significant contribution in the total event rate in the detector. However, the most important contribution is from the CXB leaking through the collimators and support structure, because these are designed only up to 150 keV which is the primary spectroscopic energy range of CZTI. We use the hard X-ray spectra of the CXB reported by Turler et al. [22] to calculate both these contributions. The contribution of the CXB within the FOV is calculated using the same method as for the source with detection efficiency of 5 mm CZT and is found to be $\sim 0.0012 \text{ cnt cm}^{-2} \text{ s}^{-1}$ in 100 keV to 300 keV. The contribution of CXB outside the FOV is calculated for two sides of CZTI as the other two sides are shielded by other instruments. Further, this contribution is also expected to be different in different CZTI modules because all modules are collimated by 0.2 mm thick Tantalum wall and hence the inner modules has increased shielding of the collimators of the outer modules. This contribution is calculated using (6).

$$N_{CXB}^{OFF} = \int_{\phi} \int_{\theta > 6^\circ} \int_{E > 100 \text{ keV}} I(E) A_{eff} T(E, \theta, \phi) \epsilon(E, \theta) d\Omega \quad (6)$$

where, $I(E)$ is hard CXB spectra [22] in $cm^{-2}s^{-1}sr^{-1}$. $d\Omega = \sin\theta d\theta d\phi$ is the solid angle. $A_{\text{eff}} = A \cos\theta$ is the effective area of the CZTI module. $T(E, \theta, \phi)$ is the transmission probability of Ta collimator(s). Total thickness of Ta, a photon (energy, E) has to pass through to reach a particular module depends on the module position, angle θ and ϕ . $\epsilon(E, \theta)$ is the detection efficiency of CZT at energy E ; effective thickness of CZT and thus efficiency of CZT depends on the angle θ . Other support structure made of Aluminum (total thickness of ~ 5 mm) is assumed to be fully transparent for this calculation. We estimated the CXB events for all the modules with average value of $\sim 0.0189 \text{ cnt } cm^{-2}s^{-1}$ in 100 keV to 300 keV. Thus the total count rate due to both the CXB within FOV and outside FOV is found to be $0.0201 \text{ cnt } cm^{-2}s^{-1}$.

5.2.2 Background due to chance coincidence

The chance coincidence can be either between two background events or a background event and source photon or even between two independent source photons. The rate of such spurious chance coincidence events can be estimated from the Poisson's distribution for the total event rate, $N \text{ cm}^{-2}s^{-1}$, in the detector which includes the source count rate, instrumental background rate and the cosmic X-ray background count rate. We estimate total count rate for an on axis source as mentioned earlier, however now using total interaction efficiency of the detector instead of the polarimetric efficiency. Source photons being detected in CZTI will depend on source strength and is found to be $\sim 0.0322 \text{ cnt } cm^{-2}s^{-1}$ in 100 keV to 300 keV for 1 Crab source intensity.

The instrumental background generally arises due to the secondary particles generated from the interaction of the high energy cosmic rays with the overall instrument as well as spacecraft material. During normal operation, most of the experimental background is expected to be flagged by anti-coincidence unit and hence rejected. However, for the purpose of calculating chance coincidence, we consider the actual counts detected in the CZT detectors. Accurate estimation of instrumental background typically requires simulation with full mass model of the spacecraft which is beyond the scope of this paper. Hence, here we use an indicative value based on our earlier HEX experiment onboard Chandrayaan-1 mission. This experiment used similar CZT modules and the observed background rate was $2 - 3 \text{ cnt } cm^{-2}s^{-1}$ [26]. Based on this, but considering different space craft structure and orbit for Astrosat, here we assume a very conservative value of $\sim 10 \text{ cnt } cm^{-2}s^{-1}$ for the instrumental background.

Based on these considerations, the total event rate, N , in the CZT detector is expected to be $\sim 10.0523 \text{ cnt } cm^{-2}s^{-1}$ in 100 keV to 300 keV for 1 Crab source strength ($0.0322 \text{ cm}^{-2}s^{-1}$ from source, $10.0 \text{ cm}^{-2}s^{-1}$ from instrumental background and $0.0201 \text{ cm}^{-2}s^{-1}$ from CXB). For this event rate, the total chance coincidence rate i.e. two events occurring within the coincidence time widow, $\Delta T = 40 \mu s$ in two adjacent pixels can be estimated using (7),

$$R_{\text{bkg}}^{\text{chance}} = \frac{(N a \Delta T)^2}{2!} e^{-N a \Delta T} N a \times N_{\text{dbl-pix}} \times 64 \quad (7)$$

where ‘a’ is twice the single pixel area (A_{pix}) and $N_{dbl-pix}$ is the total number of unique combinations of two adjacent pixels for one CZTI module. From the simple geometric considerations $N_{dbl-pix}$ is found to be 926 (i.e. 15 combinations for a single row and total 16 rows, 15 combinations for single column and total 16 columns similarly for the two diagonal directions). To get chance events for whole detector plane, the factor 64 is multiplied. The estimated chance events is $\sim 9.4055 \times 10^{-5} \text{ cnt s}^{-1}$. This value is still overestimated as we have not applied the ratio condition in the chance coincidence events. It can be seen that the chance coincidence rate is totally dominated by the instrumental background and despite assuming a very conservative value for the instrumental background, the total chance coincidence rate is extremely small as expected for a Compton polarimeter.

5.2.3 Compton scattering of CXB photons

As mentioned earlier, Compton scattering of the CXB photons constitutes a very important component of the overall polarimetric background. Again here it is necessary to consider both the CXB within the FOV of CZTI and the CXB out of the FOV. The contribution of the CXB photons in the FOV can be calculated with the same method used to estimate the source count rate, R_{src} - i.e. CXB spectra [22] multiplied with polarimetric efficiency and transparency of coded mask for 50 % obscured area and CXB spectra multiplied with only polarimetric efficiency for other 50 % unobscured area. Total rate of this component is found to be $\sim 0.0347 \text{ cnt s}^{-1}$ in 100 keV to 300 keV over the entire detector plane. Contribution to the background due to Compton scattering of out of FOV CXB photons can also be estimated using (6), however $\epsilon(E, \theta)$ has to be replaced by appropriate polarimetric efficiency for off-axis photons. We extended our Geant4 simulations for off-axis photons with incident angles ranging from 10° to 85° to estimate the efficiency of getting double pixel events satisfying all experimental conditions mentioned in previous sections. Further, this background will vary from module to module due to varying degree of shielding from the collimators of adjacent modules. We calculated the background for all diagonal modules and used an average value, found to be $\sim 1.0053 \text{ cnt s}^{-1}$, for calculating total effective background. Thus the total background due to Compton scattering of CXB is $R_{bkg}^{CXB} = 1.0400 \text{ cnt s}^{-1}$ and total background, $R_{bkg} (= R_{bkg}^{chance} + R_{bkg}^{CXB})$, affecting the overall polarimetric sensitivity, is found to be $1.0401 \text{ cnt s}^{-1}$ in 100 keV to 300 keV over the entire detector plane.

It can be seen that the total background is completely dominated by the Compton scattering of the out of FOV CXB photons. Since there is no way to distinguish between the double pixel events due to Compton scattering of genuine source photons and due to CXB photons, the large background from CXB also degrades the modulation due to scattering of the source photons. To incorporate this effect, we degrade the simulated azimuthal distribution for 100 % polarized beam, i.e. flatten it in the proportion to the total polarimetric background expected in each azimuthal bin, assuming that the azimuthal distribution of the CXB photons does not have any intrinsic modulation. Effective modulation factor is then calculated from this degraded azimuthal distribution.

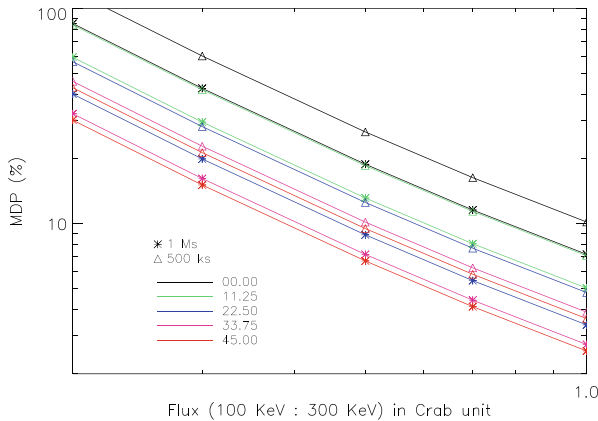


Fig. 16 Minimum Detectable Polarization (MDP) as a function of source intensity and polarization angle. MDPs are estimated for exposure times of 1 Ms (asterisks) and 500 ks (triangles)

5.3 Results

Sensitivity of CZTI in terms of the minimum detectable polarization (MDP) for a Crab like source is estimated using spurious event rate and degraded modulation factors at two different exposure times 1 Ms and 500 ks. Figure 16 shows the MDP in the energy range of 100 keV to 300 keV as a function of source intensity in Crab units.

Since, the modulation factor depends on the angle of polarization, sensitivity of the instrument is also polarization angle dependent. For a Crab like source, expected MDP is 4 to 10 % in 500 ks exposure when the polarization angle with respect to the instrument reference is 45° or 135° and 0° or 90° respectively. MDP values for different source intensities (Crab unit) and different time exposures (1 Ms and 500 ks) are shown in Table 1.

It can be seen that the polarimetric sensitivity of the Astrosat-CZTI is mainly limited due to the off-axis background because the collimators and other support

Table 1 Polarimetric Sensitivity of CZTI

| Source intensity (Crab) | Time exposure | MDP (%) |
|-------------------------|---------------|-------------|
| 0.3 | 1 Ms | 15.0 – 42.5 |
| | 500 ks | 21.0 – 60.0 |
| 0.5 | 1 Ms | 6.7 – 19.0 |
| | 500 ks | 9.5 – 26.5 |
| 0.7 | 1 Ms | 4.0 – 11.5 |
| | 500 ks | 5.5 – 16.0 |
| 1.0 | 1 Ms | 2.5 – 7.0 |
| | 500 ks | 3.5 – 10.0 |

structures are designed for the primary spectroscopic range upto 150 keV only. However, it still has significant sensitivity to reach up to the minimum detectable polarization of $\sim 5\%$ for the bright Galactic X-ray sources. Thus CZTI should be able to provide polarimetric measurements of at least 5 – 10 sources, including any new transients observed during the life time of Astrosat.

The transparent support structure, however, can be used for advantage by attempting polarimetry of off-axis bright X-ray sources or transient events such as gamma-ray bursts. Particularly in the case of GRBs, it might be more helpful to keep the lower energy threshold of 35 keV, so as to get higher modulation factor. The increased polarimetric threshold of ~ 150 keV will not result in significant degradation of the sensitivity due to the intrinsically hard spectrum of GRBs, whereas the rejection of the escape events will enhance the modulation due to the intrinsic polarization in the GRB photons available within the short duration. This can be readily done during the data analysis and does not require any change in observation mode. We plan to carry out detailed Geant4 simulations for the off axis and out of the field of view sources to estimate their impact on the polarimetric sensitivity as well as to investigate the prospects of GRB polarimetry with Astrosat-CZTI.

6 Summary

The Astrosat-CZTI, having a large detector plane with total active area of 1024 cm² and 5 mm thick CZT detectors, can provide X-ray polarization measurement at energies >100 keV. Our experiment with the CZTI detector modules confirms that these modules do have capability to record simultaneous multi-pixel events. The results of our detailed Geant4 simulations show that the CZTI will certainly have meaningful polarimetric sensitivity in the energy range of 100 keV to 250 keV, with MDP better than 10 % for a Crab like source for exposure time of 500 ks. To further confirm the polarimetric capability of complete CZTI including onboard data processing, we repeated the same experiment with partially polarized beam in the energy range of 190 keV to 240 keV and using the complete CZTI processing electronics. The partially polarized beam was generated from the scattering of 356 keV X-rays from ¹³³Ba radioactive source. Initial results of this experiment are very encouraging and confirm that the final flight configuration of CZTI will also have polarimetric capability. The experimentally measured modulation factor is slightly less than the one estimated from the Geant4 simulations, however, this is expected as the experiment uses partially polarized beam. To confirm this, we are conducting further Geant4 simulations of the actual experimental configuration. Results of the further systematic experiments with different polarization plane of the incident beam as well as associated Geant4 simulations will be reported elsewhere. However, our present experiments and simulations confirm that Astrosat-CZTI will certainly have significant polarimetric capabilities for bright Galactic X-ray sources and is likely to be the most sensitive X-ray polarimeter in this energy range. Thus, in absence of any dedicated X-ray polarimeter in near future, Astrosat-CZTI will expand the relatively unexplored field of X-ray polarimetry.

Acknowledgements Research at Physical Research Laboratory, Ahmedabad is supported by the Department of Space, Government of India. The authors thank the technical assistance provided by the CZT-Imager team at TIFR as well as at IUCAA.

References

1. Agrawal, P.C.: A broad spectral band Indian astronomy satellite Astrosat. *Adv. Space Res.* **38**, 2989–2994 (2006)
2. Bloser, P.F., Legere, J.S., McConnell, M.L., Macri, J.R., Bancroft, C.M., et al.: Calibration of the gamma-ray polarimeter experiment (GRAPE) at a polarized hard X-ray beam. *NIMPA* **600**, 424–433 (2009)
3. Chattopadhyay, T., Vadawale, S.V., Pendharkar, J.: Compton polarimeter as a focal plane detector for hard X-ray telescope: sensitivity estimation with Geant4 simulations. *Exp. Astron.* **35**, 391–412 (2013)
4. Costa, E., Soffitta, P., Bellazzini, R., Brez, A., Lumb, N., et al.: An efficient photoelectric X-ray polarimeter for the study of black holes and neutron stars. *Nature* **411**, 662–665 (2001)
5. Dean, A.J., Clark, D.J., Stephen, J.B., McBride, V.A., Bassani, L., et al.: Polarized gamma-ray emission from the Crab. *Science* **321**, 1183 (2008)
6. Geant4 Collaboration, Agostinelli, S., Allison, J., Amako, K., et al: Geant4-a simulation toolkit. *NIMPA* **506**, 250–303 (2003)
7. Gowen, R.A., Cooke, B.A., Griffiths, R.E., Ricketts, M.J.: An upper limit to the linear X-ray polarization of SCO X-1. *MNRAS* **179**, 303–310 (1977)
8. Griffiths, R.E., Ricketts, M.J., Cooke, B.A.: Observations of the X-ray nova A0620-00 with the Ariel V crystal spectrometer/polarimeter. *MNRAS* **177**, 429–440 (1976)
9. Guo, Q., Beilicke, M., Garson, A., Kislak, F., Fleming, D., et al.: Optimization of the design of the hard X-ray polarimeter X-Calibur. *Astropart. Phys.* **41**, 63–72 (2013) doi:[10.1016/j.astropartphys.2012.11.006](https://doi.org/10.1016/j.astropartphys.2012.11.006)
10. Harrison, F.A., Craig, W.W., Christensen, F.E., Hailey, C.J., Zhang, W.W., et al.: The Nuclear Spectroscopic Telescope Array (NuSTAR) high energy X-ray emission. *ApJ* **770**, 103–121 (2013)
11. Heitler, W.: *The Quantum Theory of Radiation*, 3rd edn. Oxford University Press, Oxford (1954)
12. Hughes, J.P., Long, K.S., Novick, R.: A search for X-ray polarization in cosmic X-ray sources. *ApJ* **280**, 255–258 (1984)
13. Jahoda, K.: The gravity and extreme magnetism small explorer. In: *Proceedings SPIE Conference*, vol. 7732 (2010)
14. Krawczynski, H., Garson, A., Guo, Q., Baring, M.G., Ghosh, P., et al.: Scientific prospects for hard X-ray polarimetry. *Astropart. Phys.* **34**, 550–603 (2011)
15. Laurent, P., Rodrigues, J., Wilms, J., Cadolle Bel, M., Pottschmidt, K., et al.: Polarized gamma-ray emission from the galactic black hole Cygnus X-1. *Science* **332**, 438 (2011)
16. Lei, F., Dean, A.J., Hills, G.L.: Compton polarimetry in gamma-ray astronomy. *Space Sci. Rev.* **82**, 309–388 (1997)
17. Nandi, A., Palit, S., Debnath, D., Chakrabarti, S.K., Kotoch, T.B., et al.: Instruments of RT-2 experiment onboard CORONAS-PHOTON and their test and evaluation III: coded aperture mask and Fresnel Zone Plates in RT-2/CZT payload. *Exp. Astron.* **29**, 55–84 (2011)
18. Novick, R., Weisskopf, M.C., Berthelsdorf, R., Linke, R., Wolff, R.S.: Detection of X-ray polarization of the Crab nebula. *ApJL* **174**, L1 (1972)
19. Orsi, S. et al.: POLAR: A space-borne X-Ray polarimeter for transient sources. *ASTRA* **7**, 43–47 (2011)
20. Silver, E.H., Weisskopf, M.C., Kestenbaum, H.L., Long, K.S., Novick, R., et al.: The first search for X-ray polarization in the Centaurus X-3 and Hercules X-1 pulsars. *ApJ* **232**, 248–254 (1979)
21. Soffitta, P., Costa, E., Muleri, F., Campana, R., Del Monte, E., et al.: A set of x-ray polarimeters for the new hard X-ray imaging and polarimetric Mission. In: *Proceedings SPIE Conference*, vol. 7732 (2010)

22. Turler, M., Chernyakova, M., Courvoisier, T., Lubinski, P., Neronov, A., et al.: INTEGRAL hard x-ray spectra of the cosmic x-ray background and galactic ridge emission. *Astron. Astrophys.* **512**, 181 (2010)
23. Vadawale, S.V., Chattopadhyay, T., Pendharkar, J.: A conceptual design of hard X-ray focal plane detector for simultaneous x-ray polarimetric, spectroscopic, and timing measurements. In: *Proceedings SPIE Conference*, vol. 8443 (2012)
24. Vadawale, S.V., Hong, J.S., Masui, H., Grindlay, J.E., Williams, P., et al.: Multipixel characterization of imaging CZT detectors for hard x-ray imaging and spectroscopy. In: *Proceedings SPIE Conference*, vol. 5540 (2004)
25. Vadawale, S.V., Purohit, S., Shanmugam, M., Acharya, Y.B., Goswami, J.N., et al.: Characterization and selection of CZT detector modules for HEX experiment onboard Chandrayaan-1, Vol. 598, pp. 485–495 (2009)
26. Vadawale, S.V., Sreekumar, P., Acharya, Y.B., Shanmugam, M., Banerjee, D., et al.: Hard X-ray continuum from lunar surface: results from high energy X-ray spectrometer (HEX) onboard Chandrayaan-1. In: *Advances in Space Research*. Accepted for Publication (2014). doi:[10.1016/j.asr.2013.06.013](https://doi.org/10.1016/j.asr.2013.06.013)
27. Weisskopf, M.C., Silver, E.H., Kestenbaum, H.L., Long, K.S., Novick, R.: A precision measurement of the X-ray polarization of the Crab nebula without pulsar contamination. *ApJL* **220**, L117–L121 (1978)
28. Yonetoku, D., Murakami, T., Masui, H., Kodaira, H., Aoyama, Y., et al.: Development of polarimeter for gamma-ray bursts onboard the solar-powered sail mission. In: *Proceedings SPIE Conference*, vol. 6266 (2006)